Entrapment of pusher and puller bacteria near a solid surface

Kuan-Ting Wu, Yi-Teng Hsiao, and Wei-Yen Woon
Department of Physics, National Central University, Jungli 32054, Taiwan, Republic of China

(Received 22 March 2018; published 26 November 2018)

The origin of entrapment of microswimmers near a solid surface is investigated experimentally. We report observations on cell entrapment of pusher, puller, and bimodal *Vibrio alginolyticus* near a glass surface in a custom made microchannel. We find that all the investigated bacterial strains can be entrapped near surface, regardless of their swimming modes. Furthermore, the near-surface cell concentration of pushers is reduced, while more significant entrapment was observed for pullers as the swimming speed increases. Interestingly, for the bimodal bacterial strain that could switch from pusher to puller through a reversed rotation of the flagellum, the near-surface entrapment appears to have no dependence on swimming speed. We propose a qualitative explanation to the observation, based on forces balance between steric, near-field, and dipolar-field hydrodynamic interactions.

DOI: 10.1103/PhysRevE.98.052407

I. INTRODUCTION

It is known that in fluid dynamics, motions are dominated by viscous dissipation instead of inertia under low Reynolds number condition. Evolutionally, for microbes that live in aqueous environment, termed as microswimmers, nonreciprocal motions have been developed because low Reynolds number fluid dynamics is the dominating physics law due to their small characteristic length scale [1]. Furthermore, the small length scale of the microbes also means fluctuations from the aqueous environment could easily affect their motions. Therefore, microswimmers have been regarded as model active Brownian particles in recent decades [2]. Their swimming behavior is often significantly affected in the presence of solid surfaces. Spermatozoa swimming in the female reproductive tract [3], synthetic or artificial microdevices progressing in microchannel or vessels [4], and bacteria swimming in circular trajectories near surfaces [5], are a few good examples. One of the outstanding consequences from the modification of swimming patterns is entrapment of microswimmers, such as motile swimming bacteria near surfaces. Entrapment of bacteria near surfaces can lead to important effects in biological and environmental processes such as biofilm formation [6], biofouling of maritime vessels [7], and wound infection [8].

The processes and underlying physical mechanisms of bacteria entrapment near surfaces have been investigated in many previous studies [9–23]. Similar entrapment behaviors were found for different kinds of bacteria with different sizes [12] or swimming patterns [18], in different kinds of environments such as different surface properties [19]. In most cases, pusher-type bacteria, whose rear-mounted flagella push the cell body forward, and generate flow patterns that resemble positive force dipoles, are employed [24]. Considering only far-field hydrodynamic interaction for the positive force dipoles, force balance near no-slip surfaces requires the bacteria to align their long axis of the ellipsoidal cell bodies and swim closer along the wall. This hydrodynamic attraction was suggested as a candidate to cause the cell entrapment near surface [11]. Notably, the above far-field hydrodynamics consideration suggests that puller-type bacteria (negative force dipole) would either repel themselves away from a surface or swim perpendicularly towards a solid wall, results in unstable entrapment [25]. Besides the far-field hydrodynamic interactions, research from computer simulation showed that steric interactions and rotational diffusion are sufficient to reproduce the cell observation of higher cell concentration near a no-slip solid surfaces [12]. Based on direct momentum transfer between the bacteria and solid surfaces, a microswimmer could reach a close proximity to the surface, and align to a surface due to its elongated rod-shaped cell body, while rotational diffusion could release the bacteria by randomly changing their swimming directions. It was suggested that in a room-temperature aqueous environment, the dipolar-field hydrodynamic interactions would be overwhelmed by random rotational diffusive motions, and therefore may not be able to explain in full the observed cell entrapment behaviors [12,15,17,18]. Later experiment on bacteria entrapped near convex walls showed evidence that entrapment of bacteria on surface has hydrodynamics origin. The anisotropic shear stress from a nearby no-slip wall would reorient the bacteria to swim with their axis pointing into the surface. Balanced by the increased cross-sectional fluid drag of the rod-shaped cell body when moving forward, a stable nose-down configuration would be established. The above was suggested to be the main mechanism resulting in the entrapment [21]. More recently, observations through high-resolution holographic imaging had showed the detail of cell motions near the surface. When arriving to a surface, cells are reoriented mostly by steric contact with the wall. The cells are then entrapped by the near-field hydrodynamic couplings, and exhibit wobbling motions due to rotational diffusion [22]. Most of the previous works were done with pusher bacteria with similar swimming speed. The detailed role of dipolar flow may need to be reconsidered when the swimming patterns of microswimmers are varied [15,19,20]. In particular, the strength of the dipolar-field and near-field hydrodynamic can be greatly affected by the swimming speed of microswimmers. It would be an intriguing issue to experimentally investigate the relationship between

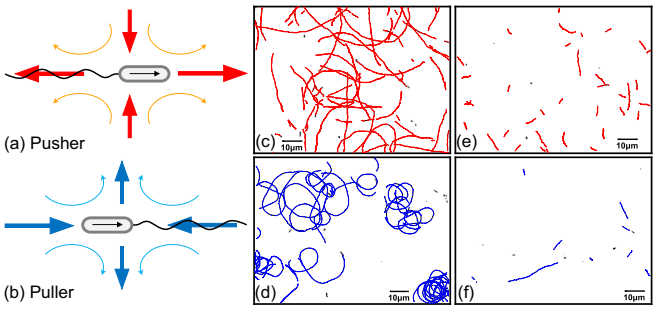

FIG. 1. Schematic illustrations for the dipolar flow (red and blue arrows) around (a) a pusher (NMB136), and (b) a puller (NMB102). Arrows inside the cells indicate the swimming direction. The trajectories (exposure time = 10 s) superposed on snapshots of the images for cell distribution in the near-surface region [z (distance from upper surface) <2 μm] for (c) pushers and (d) pullers. The trajectories taken in the open space ($z \sim 20$ μm) for (e) pushers and (f) pullers.

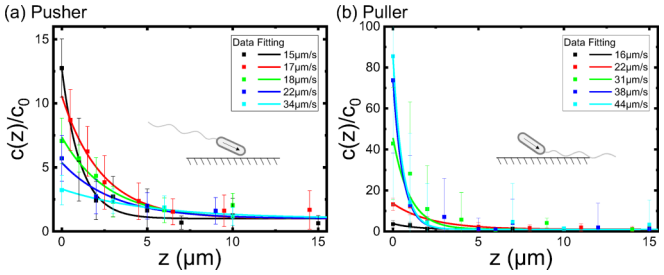

FIG. 2. Normalized cell concentration versus distance from surface, z, for (a) pushers and (b) pullers. The normalized data is fitted with an exponential function: $c(z)/c_0 = 1 + Ae^{-z/z_0}$. Solid curves are the fitting curves.

surface entrapment with respect to swimming speed. Another more intriguing issue is to see how the entrapment behaviors are modified if the pushers reverse their flagella rotation to become pullers. The above are the main focuses of this work.

II. EXPERIMENT

In this work, we measured the cell distribution of μm-sized bacteria near solid surfaces with various tunable swimming characteristics. Utilizing three different strains of *Vibrio alginolyticus*, we controlled their swimming speed through tuning sodium concentration in the aqueous medium [26–28]. These mutated ellipsoid shaped (long axis $\sim$3 μm, short axis $\sim$1 μm) bacterium is propelled by its single left-handed chiral polar flagellum (length $\sim$6 μm). NMB136 strain rotate its flagellum in counterclockwise direction, so the flow pattern generated is a positive force dipole, and can be regarded as pusher [Fig. 1(a)]. On the other hand, NMB102 rotates its flagellum in clockwise direction and can be regarded as puller [Fig. 1(b)]. We experimentally study the entrapment behaviors near surface for pushers and pullers with identical cell-flagellum structure under different swimming speed. We find that both pushers and pullers can be entrapped near surface. Furthermore, while the entrapment behaviors are strongly dependent on the swimming speed for both strains, the details are vastly different. It is found that the near-surface cell concentration of pushers is reduced as the swimming speed increases. While for pullers, more significant entrapment was observed as the swimming speed increases. Interestingly, for mutant bimodal *Vibrio alginolyticus* bacteria strain that could switch from pusher to puller through a reversed rotation of the flagellum (VIO5), the near-surface entrapment appear to have no dependence on swimming speed.

Three strains of bacteria were incubated by standard protocols shown in the Appendix. To tune their swimming speed in the experiment, bacteria were diluted into motility buffers mixed with different NaCl/KCl ratio, in order to conserve the overall ion concentration while changing the Na^+ concentration. The final bacteria concentration is $\sim 10^{14}$ cell/m^3. The main observation system was an upright bright field microscope (Olympus BX51) with an oil-immersion objective (Olympus 60×, N.A.= 1.25). The dilute bacteria suspension was observed in a custom-made microchannel built with plasma-cleaned glass slide and a cover glass spacing by double-side tapes (3M Scotch) of thickness $\sim$100 μm. As a result, there is approximately 10 cell per view in the open space. The images were recorded by a charged coupled device (CCD) camera (AVT Stingray F-033c, 60 frames per second). Using a xyz micropositioning stage (Tanlian), the cell concentration at each position away from the surface can be recorded. Averaging the number of swimming cells at speed faster than one body length in each frame by a home-built particle tracking algorithm (to further eliminate the probability of counting the nonmotile bacteria), we recorded a 30 s video at certain distances from the top surface with a focal depth of $\sim$2 μm. It is assumed that the counted number of trajectories is proportional to the cell concentration. The steady-state distribution of swimming bacteria within 20 μm away from the upper surface of the channel only is recorded to eliminate the sedimentation effect caused by gravity on the nonmotile cells. Figures 1(c) and 1(d) show the trajectories superposed on snapshots of the images for cell distribution in the near-surface region [z (distance from upper surface) <2 μm] for pushers and pullers, respectively. While Figs. 1(e) and 1(f) show the trajectories in open space ($z \sim 20$ μm), for pushers and puller, respectively. Two apparent observations can be made. First, the cell concentration is higher near surface, second, the trajectories near surface become more circularlike due to the drag from the no-slip boundary, similar to previous finding [5]. The above observations indicate typical near-surface entrapment.

The collected cell concentration data $c(z)$ were first normalized by the cell concentration at open space c_0. Figures 2(a) ad 2(b) show the normalized cell concentration versus z for pushers and pullers, respectively. It is apparent that both pushers and pullers can be entrapped at the surface. The data are fitted with an exponential function: $c(z)/c_0 = 1 + Ae^{-z/z_0}$. $1 + A$ indicates the unitless relative cell concentration closest to the surface, while z_0 in the exponent indicates the characteristic decay length. Figures 3(a) and 3(b) show the dependence of the unitless relative cell concentration $1 + A$ versus swimming speed for pushers and pullers, respectively. For pushers, $1 + A$ decays as swimming speed increases. In contrast, for pullers, $1 + A$ increases as swimming speed increases. The data can be fitted by linear curves with negative slope for pushers, and positive slope for

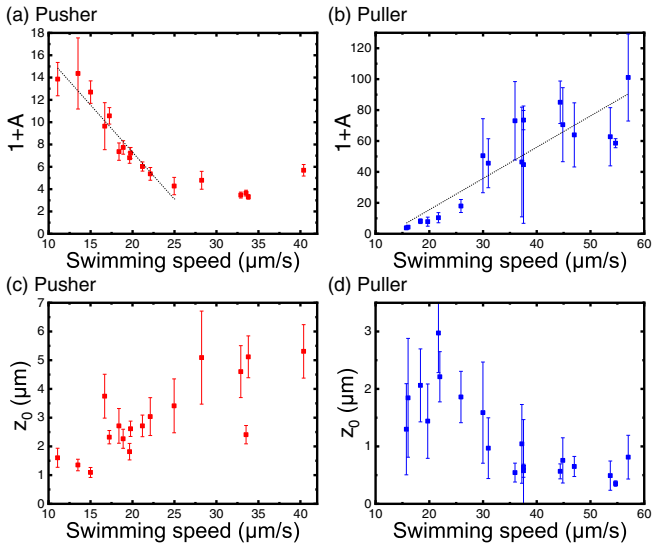

FIG. 3. (a) The fitted entrapment amplitude $1 + A$ versus swimming speed for (a) pushers, and (b) pullers. The dashed lines are the linear fitting results. The slope is $-0.84(\mu m^{-1})$ and $+1.98(\mu m^{-1})$ for (a) pushers and (b) pullers, respectively. (c) Fitted decay length z_0 versus swimming speed for (c) pushers, and (d) pullers.

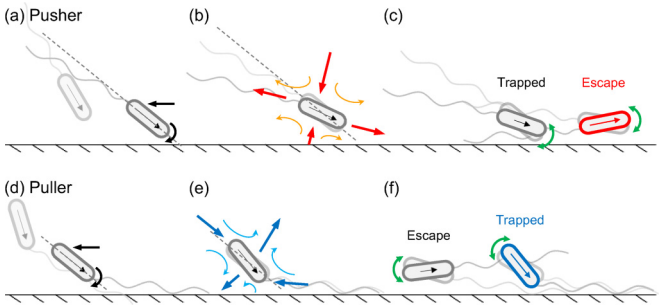

FIG. 4. Schematic illustrations for the competition among interactions when a swimming bacterium approaching a surface. Steric interaction and boundary drag leads to a tilting angle (dash lines) for swimming rod-shape bacteria for both (a) pusher and (d) puller. Taking dipolar flow into concern, the equilibrium tilting angle of a microswimmer tends to be smaller for (b) pusher and larger for (e) puller, depending on the swimming speed. In the presence of rotational diffusion, probability for a swimmer to escape is determined by its final tilting angle for both (c) pushers and (f) pullers. The length of the arrows in the cells indicate the swimming speed of the microswimmer. Overall speaking, fast pushers and slow pullers have higher chance to escape.

pullers. Distributions of the pusher swimmers generally decay slowly from the surface with $6\ \mu m > z_0 > 1\ \mu m$. The faster the bacteria swim the slower the cell concentration decays [Fig. 3(c)]. For pullers, the characteristic decay length decreases as swimming speed increases, with $3\ \mu m > z_0 > 0\ \mu m$ [Fig. 3(d)]. Generally, the concentration of pullers decreases faster with distance from the surface.

The data above suggests that (i) Near-wall interactions play significant roles: Similar to pushers, pullers can be entrapped by solid surface, despite the repulsive forces from far-field hydrodynamics, (ii) Different results from different types of swimmers as dipolar-field varies: Entrapment of pushers is weaker when the bacteria swim faster, indicating that there should be stronger counterforces that suppress entrapment of pushers on surface by the near-field hydrodynamic interactions. On the other hand, entrapment of pullers is stronger as swimming speed increases, indicating that the counterforces involved in entrapment is swimming direction dependent, i.e., the involved counterforces may orient the swimmers in directions favoring escape from surface or entrap them on surface, depending on their swimming directions. Regardless of pullers or pushers, the reaction forces from random collision of swimmers should increase in similar fashion as swimming speeds increase, thus it may not be the probable candidate for the counterforce that is involved in the observed entrapment effects. Consider similar distribution of random fluctuation of cell orientations for both strains under each condition, the only probable source for the counterforces should be the dipolar-field interactions between cells and wall.

In light of the above observations, we propose a qualitative explanation for the observed microswimmer entrapment near solid surface, suitable for both pushers and pullers. Consider a pusher that incidentally swims towards a surface with oblique angle [Fig. 4(a)]. The steric interaction from collision between the cell body and the solid wall results in a reorientation of cell that may tilt the cell body parallel to the surface. While for the near-field interaction, the viscous torque due to no-slip boundary drag tilts the cell body to orientate towards the surface at a constant angle. On the other hand, the positive dipolar hydrodynamic force from the pusher would always tend to orient the long axis of the cell body parallel to the surface [Fig. 4(b)]. The final tilting angle of the cell body relative to the surface is determined by the balance between the dipolar-field forces and boundary drag. It is expected that under faster swimming speed, the propensity for the cell to be parallel to the surface would be greater, since the dipolar field would help stabilizing the long axis of the cell parallel to surface. Consequently, the probability for the rotational diffusion to reorient the cell body direction away from surface also become greater [Fig. 4(c)]. The above qualitative explanation could explain empirically the data for pushers ($1 + A$ decreases as swimming speed increases). It also explains why for pusher the characteristic decay length z_0 increases as swimming speed increases, since the far-field hydrodynamic force is the more dominant factor.

This above model can also describe the entrapment of puller swimmers. Similar to pusher, steric and near-field hydrodynamic interactions between the swimming puller and the surface first leads to a small tilting angle [Fig. 4(d)]. Moreover, the negative dipolar hydrodynamic field from a puller tends to orientate the long axis of the cell body perpendicular to the surface [Fig. 4(e)]. The tilt angle becomes greater as the cell swimming speed increases. Note that in puller case, the swimming direction of the cell is backward so that the flagellum-down position of cells in fact result in stuck of the cell at surface. Thus, the probability for the rotational diffusion to reorient the cell away from the surface is lower at high swimming speed [Fig. 4(f)]. Nevertheless, the entrapment only happens when a microswimmer swims close enough to the surface, where the near-field hydrodynamic

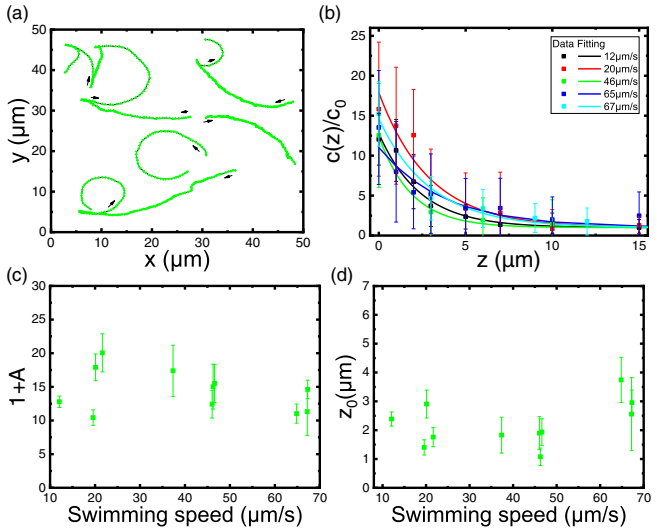

FIG. 5. (a) The trajectories of VIO5 near surface ($z < 2$ μm, exposure time = 3 s) (b) Normalized cell concentration versus distance from surface for the bimodal VIO5. (c) $1 + A$ versus swimming speed. (d) Fitted decay length z_0 versus swimming speed.

interaction can tilt it down first. While it can still happen randomly, the probability for a puller to get close enough to surface, whose negative dipolar hydrodynamic flow field tends to repel it from surface, is lower than the probability for pusher. Consequently, $1 + A$ increases and z_0 decreases as swimming speed increases.

A wild-type *Vibrio alginolyticus* can switch their swimming mode frequently between pusher and puller, known as the run-and-reverse motion [Fig. 5(a)] [27,31]. Here, we present our observation on the surface entrapment of bimodal-swimming strain (VIO5). The observation shows that bimodal bacteria can also be trapped on a surface. However, the cell distribution seems to be indifferent to the swimming speed [Fig. 5(b)]. Based on the descriptive model proposed above, it could be understood that both the positive and negative dipolar hydrodynamic forces are in play to destabilize or stabilize the cell entrapment for the bimodal VIO5. The indifference to swimming speed (Na^+ concentration) for the wild-type *Vibrio alginolyticus* may be favorable in term of evolution since the fluctuation in the salt concentration in sea water does not affect the surface entrapment behaviors.

III. CONCLUSION

In conclusion, we report observations on cell entrapment of pusher, puller, and bimodal *Vibrio alginolyticus* near a solid surface. We find that both pushers and pullers can be entrapped near surface. It is found that the near-surface cell concentration of pushers is reduced as the swimming speed increases. While for pullers, more significant entrapment was observed as the swimming speed increases. Interestingly, for bimodal *Vibrio alginolyticus* bacteria strain that could switch from pusher to puller through a flick of the flagellum, the near-surface entrapment appears to have no dependence on swimming speed. We propose a qualitative explanation to the observation based on forces balance between steric, near-field, and dipole-field hydrodynamic interactions.

ACKNOWLEDGMENT

The *Vibrio alginolyticus* strains were a kind gift from C. J. Lo [29,30].

APPENDIX A: CELL CULTURE

Three mutated strains of bacteria, NMB136, NMB102, and VIO5, can be cultured in the same way. First, to increase the population, 2.5 μl, $-20\,^{\circ}$C frozen *Vibrio* aliquot suspending in a test tube of 1 ml VC growth medium is incubated overnight for around 13 h. (VC: 0.5% polypeptone, 0.5% yeast extract, 0.4% potassium phosphate dibasic, 3.0% sodium chloride, 0.2% glucose) After that, to enhance the bacteria motility, 1 ml VPG medium is added into 10 μl overnight broth, and incubated for another 3 $\sim$ 5 hours. (VPG: 1.0% polypeptine, 0.4% potassium phosphate dibasic, 3.0% sodium chloride, 0.5% glycerol). When the optical density (OD600) of the bacteria suspension reaches $\sim$0.6, we centrifuge 40 μl of the suspension for 5 min at $\sim$1800 rcf(g). Then, the sediment is resuspended in 200 μl TMN motility buffer, where the sodium concentration can be tuned by the ratio of added NaCl and KCl. (TMN: pH 7.5, comprising 50 mM Tris-HCl, 5mM magnesium chloride and glucose respectively, and 500 mM of KCl/NaCl) This diluted bacteria suspension will be injected into a microchannel.

APPENDIX B: BACTERIA TRACKING

To exclude the nonmotile bacteria when observing the accumulation of bacteria near surfaces, we tracked and counted swimming bacteria in certain distances from surfaces. A home-built C++ program with OpenCV library was used to analyze the recorded videos. We first translated the video into grayscale images [Fig. 6(a)], which represent only the intensity of light at each pixel by shades of gray, changing between black (the weakest 0) and white (the strongest 255). After the translation, we picked the upper and lower thresholds of the intensity, where the bacteria in the focal plane were highlighted (normally 145 $\sim$ 225 in our system). Setting the picked pixels black and the others white, the projection of the bacteria remains [Fig. 6(b)]. We calculate the centroid of each bacteria projections. A semi-two-dimensional trajectory of a bacterium can be plotted by linking the nearest centroids in the following images [Fig. 7]. From the sequence of the bacteria centroid positions, swimming speed and mean-square displacement of each bacterium can be calculated for the

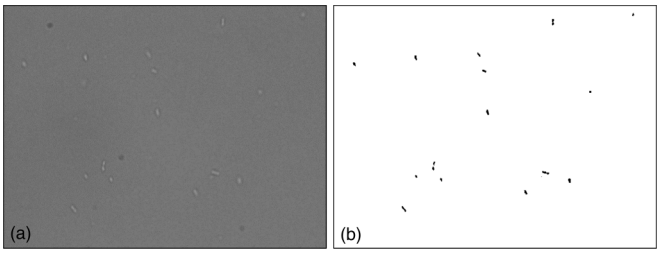

FIG. 6. (a) Grayscale image from a video (b). The digitalized image after thresholding.

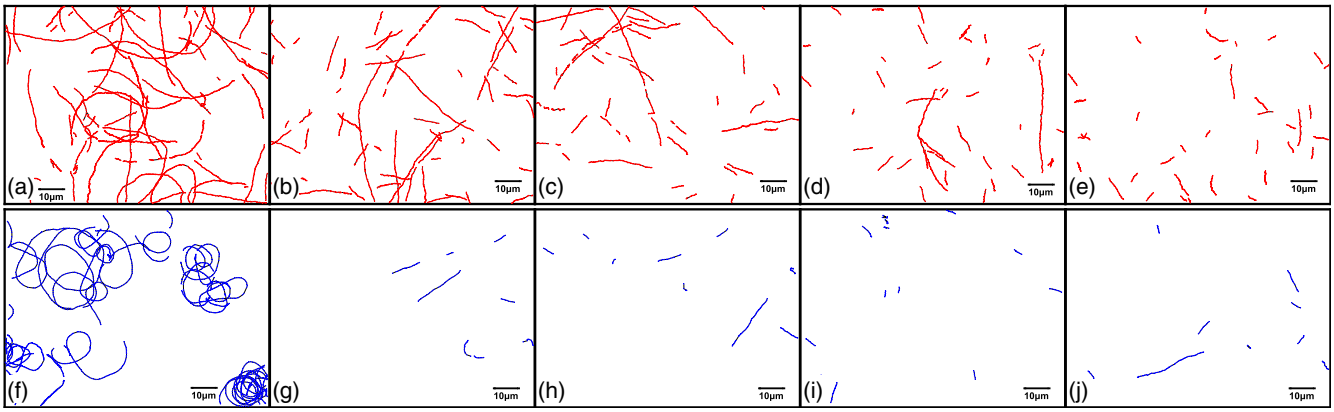

FIG. 7. Recorded bacteria trajectories (a)–(e) for pushers and (f)–(j) for pullers at (correspondingly left to right) $<2\ \mu$m, 4 μm, 6 μm, 10 μm, 20 m away from the upper surface. Bacteria centroids (red and blue symbols) were linked by black lines individually. Converse circular motions of (a) pushers and (f) pullers were recorded, while both swimmers tend to swim straight in bulk (e), (j).

following analysis. Only normally swimming bacteria are counted when observing the cell distribution.

Figure 7 shows the bacteria trajectories captured in 10 s at $<2\ \mu$m, 4 μm, 6 μm, 10 μm, 20 m (left to right) away from the upper surface. Distinct cell distribution near a wall can be observed. Pushers ($\sim$17 m/s) accumulate and decay slowly from the surface [Figs. 7(a)–7(e)], while pullers ($\sim$45 m/s) were trapped on the surface for longer time or kept themselves away (rapidly decay) [Figs. 7(f)–7(j)].

Another remarkable feature of flagellated bacteria swimming near surfaces is the circular motions, as a result of the rotation of the flagella and the cell body near a no-slip surface [10,13]. For pushers on surface [Fig. 7(a)], they tend to circulate clockwise (CW) for their flagellum spinning counterclockwise (CCW) and cell body spinning CW. And for our puller rotating their flagellum conversely [Fig. 7(f)], CCW circular motions were observed. This characteristic of swimming bacteria helps us to distinguish the identical microswimmers.

[1] E. M. Purcell, Am. J. Phys. **45**, 3 (1977).
[2] M. E. Cates and J. Tailleur, Europhys. Lett. **101**, 20010 (2013).
[3] S. S. Suarez and A. A. Pacey, Hum. Reprod. Update **12**, 23 (2006).
[4] A. T. Brown, I. D. Vladescu, A. Dawson, T. Vissers, J. Schwarz-Linek, J. S. Lintuvuori, and W. C. K. Poon, Soft Matter **12**, 131 (2016).
[5] E. Lauga, W. R. DiLuzio, G. M. Whitesides, and H. A. Stone, Biophys. J. **90**, 400 (2006).
[6] J. C. Conrad, Res. Microbiol. **163**, 619 (2012).
[7] D. M. Yebra, S. Kiil, and K. Dam-Johansen, Prog. Org. Coat. **50**, 75 (2004).
[8] T. Dalton, S. E. Dowd, R. D. Wolcott, Y. Sun, C. Watters, J. A. Griswold, and K. P. Rumbaugh, PLoS One **6**, e27317 (2011).
[9] L. Rothschild, Nature (London) **198**, 1221 (1963).
[10] T. Goto, K. Nakata, K. Baba, M. Nishimura, and Y. Magariyama, Biophys. J. **89**, 3771 (2005).
[11] A. P. Berke, L. Turner, H. C. Berg, and E. Lauga, Phys. Rev. Lett. **101**, 038102 (2008).
[12] G. Li and J. X. Tang, Phys. Rev. Lett. **103**, 078101 (2009).
[13] D. Giacché, T. Ishikawa, and T. Yamaguchi, Phys. Rev. E **82**, 056309 (2010).
[14] H. Shum, E. A. Gaffney, and D. J. Smith, Proc. R. Soc. A **466**, 1725 (2010).
[15] K. Drescher, J. Dunkel, L. H. Cisneros, S. Ganguly, and R. E. Goldstein, Proc. Natl. Acad. Sci. USA **108**, 10940 (2011).
[16] G. Li, J. Bensson, L. Nisimova, D. Munger, P. Mahautmr, J. X. Tang, M. R. Maxey, and Y. V. Brun, Phys. Rev. E **84**, 041932 (2011).
[17] S. E. Spagnolie and E. Lauga, J. Fluid Mech. **700**, 105 (2012).
[18] V. Kantsler, J. Dunkel, M. Polin, and R. E. Goldstein, Proc. Natl. Acad. Sci. USA **110**, 1187 (2013).
[19] M. Molaei, M. Barry, R. Stocker, and J. Sheng, Phys. Rev. Lett. **113**, 068103 (2014).
[20] M. Contino, E. Lushi, I. Tuval, V. Kantsler, and M. Polin, Phys. Rev. Lett. **115**, 258102 (2015).
[21] O. Sipos, K. Nagy, R. Di Leonardo, and P. Galajda, Phys. Rev. Lett. **114**, 258104 (2015).
[22] S. Bianchi, F. Saglimbeni, and R. Di Leonardo, Phys. Rev. X **7**, 011010 (2017).
[23] P. Sartori, E. Chiarello, G. Jayaswal, M. Pierno, G. Mistura, P. Brun, A. Tiribocchi, and E. Orlandini, Phys. Rev. E **97**, 022610 (2018).
[24] T. J. Pedley and J. O. Kessler, Annu. Rev. Fluid Mech. **24**, 313 (1992).
[25] E. Lauga and T. R. Powers, Rep. Prog. Phys. **72**, 096601 (2009).
[26] C. Golten and W. A. Scheffers, J. Sea Res. **9**, 351 (1975).
[27] I. Kawagishi, M. Imagawa, Y. Imae, L. McCarter, and M. Homma, Mol. Microbiol. **20**, 693 (1996).
[28] N. Li, S. Kojima, and M. Homma, Genes Cells **16**, 985 (2011).
[29] Y. T. Hsiao, J. H. Wang, Y. C. Hsu, C. C. Chiu, C. J. Lo, C. W. Tsao, and W. Yen Woon, Appl. Phys. Lett. **100**, 203702 (2012).
[30] M. Homma, H. Oota, S. Kojima, I. Kawagishi, and Y. Imae, Microbiology **142**, 2777 (1996).
[31] K. Son, J. S. Guasto, and R. Stocker, Nat. Phys. **9**, 494 (2013).